microPET Imaging of Glioma Integrin $\alpha_v\beta_3$ Expression Using ^{64}Cu-Labeled Tetrameric RGD Peptide

Yun Wu, PhD[1]; Xianzhong Zhang, PhD[1]; Zhengming Xiong, MD, PhD[1]; Zhen Cheng, PhD[1]; Darrell R. Fisher, PhD[2]; Shuang Liu, PhD[3]; Sanjiv S. Gambhir, MD, PhD[1]; and Xiaoyuan Chen, PhD[1]

[1]Molecular Imaging Program at Stanford (MIPS), Department of Radiology and Bio-X Program, Stanford University, Stanford, California; [2]Radioisotopes Program, Pacific Northwest National Laboratory, Richland, Washington; and [3]Industrial and Physical Pharmacy, School of Health Sciences, Purdue University, West Lafayette, Indiana

Integrin $\alpha_v\beta_3$ plays a critical role in tumor-induced angiogenesis and metastasis and has become a promising diagnostic indicator and therapeutic target for various solid tumors. Radiolabeled RGD peptides that are integrin specific can be used for noninvasive imaging of integrin expression level as well as for integrin-targeted radionuclide therapy. **Methods:** In this study we developed a tetrameric RGD peptide tracer ^{64}Cu-DOTA-E{E[c(RGDfK)]$_2$}$_2$ (DOTA is 1,4,7,10-tetraazacyclododecane-*N,N′,N″,N‴*-tetraacetic acid) for PET imaging of integrin $\alpha_v\beta_3$ expression in female athymic nude mice bearing the subcutaneous UG87MG glioma xenografts. **Results:** The RGD tetramer showed significantly higher integrin binding affinity than the corresponding monomeric and dimeric RGD analogs, most likely due to a polyvalency effect. The radiolabeled peptide showed rapid blood clearance (0.61 ± 0.01 %ID/g at 30 min and 0.21 ± 0.01 %ID/g at 4 h after injection, respectively [%ID/g is percentage injected dose per gram]) and predominantly renal excretion. Tumor uptake was rapid and high, and the tumor washout was slow (9.93 ± 1.05 %ID/g at 30 min after injection and 4.56 ± 0.51 %ID/g at 24 h after injection). The metabolic stability of ^{64}Cu-DOTA-E{E[c(RGDfK)]$_2$}$_2$ was determined in mouse blood, urine, and liver and kidney homogenates at different times after tracer injection. The average fractions of intact tracer in these organs at 1 h were approximately 70%, 58%, 51%, and 26%, respectively. Noninvasive microPET studies showed significant tumor uptake and good contrast in the subcutaneous tumor-bearing mice, which agreed well with the biodistribution results. Integrin $\alpha_v\beta_3$ specificity was demonstrated by successful blocking of tumor uptake of ^{64}Cu-DOTA-E{E[c(RGDfK)]$_2$}$_2$ in the presence of excess c(RGDyK) at 1 h after injection. The highest absorbed radiation doses determined for the human reference adult were received by the urinary bladder wall (0.262 mGy/MBq), kidneys (0.0296 mGy/MBq), and liver (0.0242 mGy/MBq). The average effective dose resulting from a single ^{64}Cu-DOTA-E{E[c(RGDfK)]$_2$}$_2$ injection was estimated to be 0.0164 mSv/MBq. **Conclusion:** The high integrin and avidity and favorable biokinetics make ^{64}Cu-DOTA-E{E[c(RGDfK)]$_2$}$_2$ a promising agent for peptide receptor radionuclide imaging and therapy of integrin-positive tumors.

Key Words: tumor angiogenesis; integrin; RGD peptide; microPET; multimeric peptide; ^{64}Cu

J Nucl Med 2005; 46:1707–1718

Malignant gliomas are the most common types of brain tumors and are the second leading cause of cancer death in children under 15 y old and also in young adults up to 34 y old (*1,2*). With a high proliferation rate, marked neovascularization, and extensive local invasion of tumor cells into the normal brain parenchyma, gliomas are resistant to traditional radiation and chemotherapy, which leads to patient mortality over months or years (*3*). Recent clinical and experimental evidence suggests that the tumor growth and progression are dependent on angiogenesis and invasion, which share common regulatory mechanisms (*4*). Angiogenesis is an invasive process characterized by endothelial cell proliferation, modulation of the extracellular matrix (ECM), and cell adhesion and migration (*5*). Among many angiogenic factors, the cell adhesion molecule integrin is a mediator of angiogenesis in many tumor types, including gliomas (*6*). Integrins are part of a family of heterodimeric transmembrane receptors involved in multiple steps of angiogenesis and metastasis. Integrins on endothelial cells bind to and respond to the ECM components, and this interaction is accompanied by the transduction of positional cues from the ECM to the intracellular signaling machinery (*7*). The function of these protein receptors during angiogenesis has been studied with integrin $\alpha_v\beta_3$, which is not readily detectable in quiescent vessels but becomes highly expressed in angiogenic vessels and tumor cells (*8,9*). The $\alpha_v\beta_3$ integrin is necessary for the formation, survival, and maturation of newly formed blood vessels (*10*) and its expression correlates with tumor grade and histologic type (*11*).

Received Apr. 5, 2005; revision accepted Jun. 13, 2005.

For correspondence or reprints contact: Xiaoyuan Chen, PhD, Molecular Imaging Program at Stanford (MIPS), Stanford University, 1201 Welch Rd., P095, Stanford, CA 94305-5484.

E-mail: shawchen@stanford.edu

Recent data both in preclinical tumor models and in phase I/II clinical trials suggest that antagonists of $\alpha_v\beta_3$ integrin inhibit tumor angiogenesis and metastasis (*12,13*). The ability to noninvasively visualize and quantify $\alpha_v\beta_3$ integrin expression level provides opportunities to document tumor (tumor cells and sprouting tumor vasculature) receptor expression, to more appropriately select patients considered for antiintegrin treatment, and to monitor treatment efficacy in integrin-positive patients. Several molecular probes have been developed for MRI (*14*), ultrasound (*15*), optical imaging (*16*), PET, and SPECT applications (*17*). Although most of the RGD peptide-based probes could target tumors by binding integrin $\alpha_v\beta_3$, they suffer from modest tumor uptake and unfavorable pharmacokinetics that limit their applications for imaging and internal radiotherapy.

We and others have reported radiolabeled RGD-containing peptide dimers as radiopharmaceuticals for diagnosis of rapidly growing solid tumors (*18–23*). It was hypothesized that the receptor binding of one RGD cyclic peptide will significantly enhance the "local concentration" of the other RGD peptide in the vicinity of the receptor, which may lead to a faster rate of receptor binding or a slower rate of dissociation of radiolabeled RGD dimer from the integrin $\alpha_v\beta_3$ and result in higher uptake and longer retention time in the tumor. A multimeric RGD peptide with >2 repeating cyclic RGD units is thus expected to further enhance the affinity of the receptor–ligand interactions even more significantly through the phenomenon of a polyvalency effect. The apparent increase in molecular size may also prolong circulation time of the multimer and consequently reduce tumor washout rate.

In this investigation we applied the polyvalency principle and developed a novel tetrameric RGD peptide using glutamate as the branching unit. The resulting RGD peptide tetramer was conjugated with the macrocylic chelator 1,4,7,10-tetraazacyclododecane-*N,N′,N″,N‴*-tetraacetic acid (DOTA) and labeled with ^{64}Cu for microPET imaging of integrin expression in a subcutaneous U87MG glioblastoma xenograft model in female athymic nude mice. The aim of this study was to investigate integrin targeting characteristics of ^{64}Cu-DOTA-E{E[c(RGDfK)]$_2$}$_2$ as a potential agent for diagnosis and receptor-mediated internal radiotherapy of integrin receptor–expressing tumors.

MATERIALS AND METHODS

All commercially available chemical reagents were used without further purification. DOTA was purchased from Macrocyclics, Inc. Dicyclcohexylcarbodiimide (DCC), 1-ethyl-3-[3-(dimethylamino)propyl]carbodiimide (EDC), *N*-hydroxysulfonosuccinimide (SNHS), and Chelex 100 resin (50–100 mesh) were purchased from Aldrich. Water and all buffers were passed over a Chelex 100 column (1 × 15 cm) before use in radiolabeling procedures. Reversed-phase extraction C-18 Sep-Pak cartridges were obtained from Waters. The syringe filter and polyethersulfone membranes (pore size, 0.2 μm; diameter, 13 mm) were obtained from Nalge Nunc International. ^{125}I-echistatin, labeled by the lactoperoxidase method to a specific activity of 74,000 GBq/mmol (2,000 Ci/mmol), was purchased from Amersham Biosciences. The female athymic nude mice were supplied from Harlran at 4–5 wk of age. ^{64}Cu (half-life [$t_{1/2}$] = 12.7 h, β^+ = 655 keV [17.4%], β^- = 573 keV [30%]) was obtained form Mallinckrodt Institute of Radiology, Washington University School of Medicine (St. Louis, MO). ^{64}Cu was produced in a CS-15 biomedical cyclotron using the ^{64}Ni(p,n,)^{64}Cu nuclear reaction and supplied in high specific activity as $CuCl_2$ in 0.1 mol/L of HCl. The monomeric cyclic RGD peptide, c(RGDfK), was prepared via solution cyclization of the linear peptide H-Gly-Asp(OtBu)-D-Phe-Lys(Boc)-Arg(Pbf)-OH. Trifluoroacetic acid (TFA) deprotection in the presence of the free radical scavenger triisopropylsilane produced the desired cyclic pentapeptide c(RGDfK) (*24–27*). The RGD peptide dimer E[c(RGDfK)]$_2$ was prepared according to the literature method (*18*).

Analytic as well as semipreparative reversed-phase high-performance liquid chromatography (RP-HPLC) were performed on a Dionex 680 chromatography system with a UVD 170U absorbance detector and model 105S single-channel radiation detector (Carroll & Ramsey Associates). The recorded data were processed using Chromeleon version 6.50 software. Isolation of DOTA-conjugated peptide and ^{64}Cu-labeled peptide was performed using a Vydac protein and peptide column (218TP510; 5 μm, 250 × 10 mm). The flow was 5 mL/min, with the mobile phase starting from 95% solvent A (0.1% TFA in water) and 5% solvent B (0.1% TFA in acetonitrile) (0–3 min) to 35% solvent A and 65% solvent B at 33 min. The analytic HPLC was performed using the same gradient system, but with a Vydac 218TP54 column (5 μm, 250 × 4.6 mm) and flow of 1 mL/min. Ultraviolet (UV) absorbance was monitored at 218 nm.

Preparation of Boc-Glu(OSu)-OSu

To a solution of the Boc-protected glutamic acid (0.247 g, 1.0 mmol) in 5 mL of *N,N*-dimethylforamide (DMF) were added *N*-hydroxysuccinimide (NHS) (0.253 g, 2.2 mmol) and DCC (0.453 g, 2.2 mmol). The resulting mixture was stirred at room temperature for 10 h. The dicyclohexylurea (DCU) by-product was filtered off. The filtrate was evaporated to dryness under vacuum to give a crude product, which was then taken up in 3 mL of methylene chloride. The insoluble solid was filtered off. The filtrate was concentrated to about 1 mL. The solution was added dropwise into 30 mL of ether. The desired product was precipitated as white solid, which was dried in vacuo. The yield was 0.27 g (~61%). ^{1}H NMR ($CDCl_3$) δ-5.23 (br s, 1H, NH), 4.82 (m, 1H, CH), 2.85 (m, 8H, succinimide group), 2.44–2.25 (m, 2H, CH_2CO), 1.52 (m, 2H, CH_2CH_2CO), 1.46 (s, 9H, t-Bu).

Preparation of Cyclic RGD Peptide Tetramer: E{E[c(RGDfK)]$_2$}$_2$

To a solution of the Boc-protected glutamic acid activated ester Boc-E(OSu)$_2$ (4.4 mg, 0.01 mmol) in anhydrous DMF (1 mL) was added the cyclic RGD peptide dimer E[c(RGDfK)]$_2$ (39.4 mg, 0.03 mmol). The pH of the resulting mixture was adjusted to 8.5–9.0 with diisopropylethyl amine (DIPEA). The reaction was stirred at room temperature overnight and the desired product, Boc-E{E[c(RGDfK)]$_2$}$_2$, was isolated by semipreparative HPLC. The collected fractions were combined and lyophilized to give a fluffy white powder. The yield was 15 mg (~53%). Electrospray ionization mass spectroscopy (ESI-MS) (positive mode): m/z = 2,848 for $[M + H]^+$ ($C_{128}H_{187}N_{39}O_{56}$, calculated molecular weight [MW] = 2,847). The Boc-group was readily removed by treating Boc-

$E\{E[c(RGDfK)]_2\}_2$ with anhydrous TFA for 5 min. The crude product was purified by HPLC. The collected fractions were combined and lyophilized to afford $E\{E[c(RGDfK)]_2\}_2$ as a white powder. The yield was 98%. ESI-MS (positive mode): m/z = 2,748 for $[M + H]^+$ ($C_{123}H_{181}N_{39}O_{34}$, calculated MW = 2,747).

DOTA Conjugation and ^{64}Cu Radiolabeling

DOTA-$E\{E[c(RGDfK)]_2\}_2$ was synthesized in a manner similar to that described before (*18,26,28,29*). Briefly, DOTA was activated by EDC and SNHS at pH 5.5 for 30 min with a molar ratio of DOTA:EDC:SNHS = 10:5:4. The DOTA-OSSu reaction mixture (15 μmol, calculated on the basis of SNHS) was cooled to 4°C and added to $E\{E[c(RGDfK)]_2\}_2$ (2 mg, 0.6 μmol) dissolved in 500 μL of water. The reaction mixture was adjusted to pH 8.5 with 0.1N of NaOH and was allowed to incubate overnight at 4°C. The DOTA-coupled peptide was purified by semipreparative HPLC. The peak containing the tetramer conjugate was collected, lyophilized, and dissolved in water (2 mg/mL) for use in radiolabeling reactions. The yield was 1.4 mg (~75%). Matrix-assisted laser desorption ionization time-of-flight mass spectroscopy (MALDI-TOF MS): m/z = 3,135.3 for $[M + H]^+$ ($C_{139}H_{205}N_{43}O_{41,}$ calculated MW = 3,135.5)

DOTA-$E\{E[c(RGDfK)]_2\}_2$ was radiolabeled with ^{64}Cu to obtain ^{64}Cu-DOTA-$E\{E[c(RGDfK)]_2\}_2$. In brief, $^{64}CuCl_2$ (74 MBq) was diluted in 400 μL of 0.1 mol/L sodium acetate and added to the DOTA conjugate (5 μg peptide per mCi ^{64}Cu). The reaction mixture was incubated for 1 h at 50°C. ^{64}Cu-DOTA-$E\{E[c(RGDfK)]_2\}_2$ was then purified by semipreparative HPLC. The radioactive peak containing ^{64}Cu-DOTA-$E\{E[c(RGDfK)]_2\}_2$ was collected, the solvent was evaporated, and the activity was reconstituted in phosphate-buffered saline (PBS) and passed through a 0.22-μm syringe filter for in vivo animal experiments.

Octanol–Water Partition Coefficient

Approximately 111 kBq of ^{64}Cu-DOTA-$E\{E[c(RGDfK)]_2\}_2$ in 500 μL of PBS (pH 7.4) were added to 500 μL of octanol in an Eppendorf microcentrifuge tube. The 2 layers were mixed for 5 min at room temperature, the tubes were centrifuged at 12,500 rpm for 5 min (model 5415R Eppendorf microcentrifuge; Brinkman), and 200-μL aliquots of both layers were counted in a γ-counter (Packard Instruments). The experiment was repeated 3 times.

Cell Integrin Receptor-Binding Assay

In vitro integrin-binding affinities and specificities of DOTA-conjugated RGD peptides were assessed via displacement cell-binding assays using ^{125}I-echistatin as the integrin-specific radioligand. Experiments were performed on human glioblastoma U87MG cell line by modification of a method previously described (*28*). Cells were grown in Dulbecco's medium (Gibco) supplemented with 10% fetal bovine serum (FBS), 100 IU/mL penicillin, and 100 μg/mL streptomycin (Invitrogen Co.), at 37°C in a humidified atmosphere containing 5% CO_2. During the cell-binding assay experiment, the cells were harvested, washed twice with PBS, and resuspended (2×10^6 cells/mL) in binding buffer (20 mmol/L Tris, pH 7.4, 150 mmol/L NaCl, 2 mmol/L $CaCl_2$, 1 mmol/L $MgCl_2$, 1 mmol/L $MnCl_2$, 0.1% bovine serum albumin). Filter multiscreen DV plates (96-well; pore size, 0.65 μm; Millipore) were seeded with 10^5 cells and incubated with ^{125}I-echistatin (30,000 cpm/well) in the presence of increasing concentrations of different RGD peptide analogs (0–1,000 nmol/L). The total incubation volume was adjusted to 200 μL. After the cells were incubated for 2 h at room temperature, the plates were filtered through a multiscreen vacuum manifold and washed twice with cold binding buffer. The hydrophilic polyvinylidenedifluoride (PVDF) filters were collected and the radioactivity was determined using a NaI(Tl) γ-counter (Packard Instruments). The best-fit 50% inhibitory concentration (IC_{50}) values for the U87MG cells were calculated by fitting the data by nonlinear regression using GraphPad Prism (GraphPad Software, Inc.). Experiments were performed twice with triplicate samples.

Animal Models

Animal procedures were performed according to a protocol approved by Stanford University Institutional Animal Care and Use Committee. Human brain cancer carcinoma xenografts were induced by subcutaneous injection of 10^7 U87MG cells into the right front leg of female athymic nude mice. Three weeks after inoculation of the tumor cells, when the tumor reached 0.4–0.6 cm in diameter, the mice were used for biodistribution and microPET (Concorde Microsystems Inc.) experiments.

In Vivo Metabolic Stability Studies

The metabolic stability of ^{64}Cu-DOTA-$E\{E[c(RGDfK)]_2\}_2$ was evaluated in normal athymic nude mice using the method described in the literature with some modifications (*29*). Animals were sacrificed and dissected at 30 min, 1 h, and 2 h after injection of 7.4 MBq of activity into the tail vein. Blood was immediately centrifuged for 5 min at 15,000*g*. Liver and kidneys were homogenized, extracted with 500 μL PBS, and centrifuged at 15,000*g* for 5 min. After removal of the supernatants, the pellets were washed with 1 mL PBS. For each sample, supernatants of both centrifugation steps of blood, liver, and kidneys were combined and passed through Sep-Pak C-18 cartridges. The urine sample was diluted with 1 mL PBS and passed through a C-18 cartridge. The cartridges were washed with 2 mL of water and eluted with 2 mL acetonitrile containing 0.1% TFA. After evaporation of the solvent, the residues were redissolved in 1 mL PBS. Aliquots of 400 μL were injected onto analytic RP-HPLC.

Biodistribution Studies

Female nude mice bearing tumor xenography of human glioblastoma U87MG were injected with 0.74–1.11 MBq of ^{64}Cu-DOTA-$E\{E[c(RGDfK)]_2\}_2$. The mice were sacrificed and dissected at 30 min, 1, 2, 4, and 24 h after injection of ^{64}Cu-labeled tetrameric RGD peptide. The blocking experiment was performed by coinjecting radiotracer with a saturating dose of c(RGDyK) (10 mg/kg) and sacrificed at 1 h after injection. Blood, tumor, major organs, and tissues were collected and wet weighted. The radioactivity in the tissues was measured using a γ-counter. The results are presented as the percentage injected dose per gram (%ID/g). For each mouse, the radioactivity of the tissue samples was calibrated against a known aliquot of the injectate and normalized to a body mass of 20 g. Values are expressed as mean ± SD for a group of 3 animals.

Calibration of microPET

Scanner activity calibration was performed to map between microPET image units and units of radioactivity concentration. A preweighed 50-mL centrifuge tube was filled with distilled water and $^{64}CuCl_2$ (~9.3 MBq [~250 μCi] as determined by the dose calibrator) was used to simulate the whole body of the mouse. This tube was weighed, centered in the scanner aperture, and imaged for a 30-min static image, single bed position. From the sample weight and assuming a density of 1 g/mL, the activity concentration in the

bottle was calculated in units of μCi/mL. Eight planes were acquired in the coronal section. A rectangular region of interest (ROI) (counts/pixel/s) was drawn on the middle of 8 coronal planes. Using these data, a calibration factor (C) was obtained by dividing the known radioactivity in the cylinder (μCi/mL) by the image ROI. This calibration factor was determined periodically and did not vary significantly with time.

microPET Studies

PET of tumor-bearing mice was performed on a microPET R4 rodent model scanner (Concorde Microsystems Inc.). The scanner has computer-controlled vertical and horizontal bed motion, with an effective axial field of view (FOV) of 7.8 cm and a transaxial FOV of 10 cm. U87MG tumor-bearing mice ($n = 3$) were imaged in the prone position in the microPET scanner. The mice were injected with about 9.3 MBq of ^{64}Cu-DOTA-E{E[c(RGDfK)]$_2$}$_2$ via the tail vein and then anesthetized with 2% isoflurane and placed near the center of the FOV of the microPET where the highest image resolution and sensitivity are obtained. The 10-min static scans were obtained at 15 min, 30 min and 1, 2, 4, and 18 h after injection. The images were reconstructed by a 2-dimensional ordered-subsets expectation maximum (OSEM) algorithm. No correction was necessary for attenuation and scattering. At each microPET scan, ROIs were drawn over each tumor, normal tissue, and major organs on decay-corrected whole-body coronal images. The average radioactivity concentration (accumulation) within a tumor or an organ was obtained from mean pixel values within the multiple ROI volumes, which were converted to counts/mL/min by using the calibration constant C. Assuming a tissue density of 1 g/mL, the ROIs were then converted to counts/g/min, and then divided by the administered activity to obtain an imaging ROI-derived percentage administered activity per gram of tissue (%ID/g). For a receptor-blocking experiment, mice bearing U87MG tumors on the right front leg were imaged at 1 h (10-min static scan) after administration of 9.3 MBq of ^{64}Cu-DOTA-E{E[c(RGDfK)]$_2$}$_2$ coinjected with 10 mg/kg c(RGDyK).

Radiation Dose Extrapolations to the Human

Radiation-absorbed doses were not estimated for our U87MG tumor-bearing mice. However, the mouse biodistribution data (uptake, retention, and clearance) were used to project radiation-absorbed doses that could be expected in human subjects administered ^{64}Cu-DOTA-E{E[c(RGDfK)]$_2$}$_2$. Projected radiation-absorbed doses for humans were made by assuming that, for the purpose of this exercise, the metabolism rates and pharmacokinetics of ^{64}Cu-DOTA-E{E[c(RGDfK)]$_2$}$_2$ in man and mouse were equivalent. Therefore, the biodistribution data were assumed to apply to a reference adult human subject. Time–activity curves were generated from the mean values obtained in mice for each organ of interest. We then calculated source organ residence times for the human model by integrating a monoexponential fit to the experimental biodistribution data for each organ or tissue by standard methods. The whole-body time–activity curve was integrated by fitting the whole-body retention data to a biphasic exponential decay curve, which represented the retention data more closely than a single exponential equation. The source organ residence times obtained forthwith were used with a standard quantitation platform Organ Level Internal Dose Assessment (OLINDA; Vanderbilt University) (*30*). Note that the residence time for the urinary bladder was calculated without incorporating a dynamic bladder model.

Statistical Analysis

The data were expressed as means ± SD. One-way ANOVA was used for statistical evaluation. Means were compared using the Student t test. P values < 0.05 were considered significant.

RESULTS

Chemistry and Radiochemistry

The synthesis of DOTA-E{E[c(RGDfK)]$_2$}$_2$ (Fig. 1) was performed through an active ester method by coupling Boc-Glu(OSu)-OSu with dimeric RGD peptide E[c(RGDfK)]$_2$ followed by TFA deprotection. In aqueous solution, DOTA

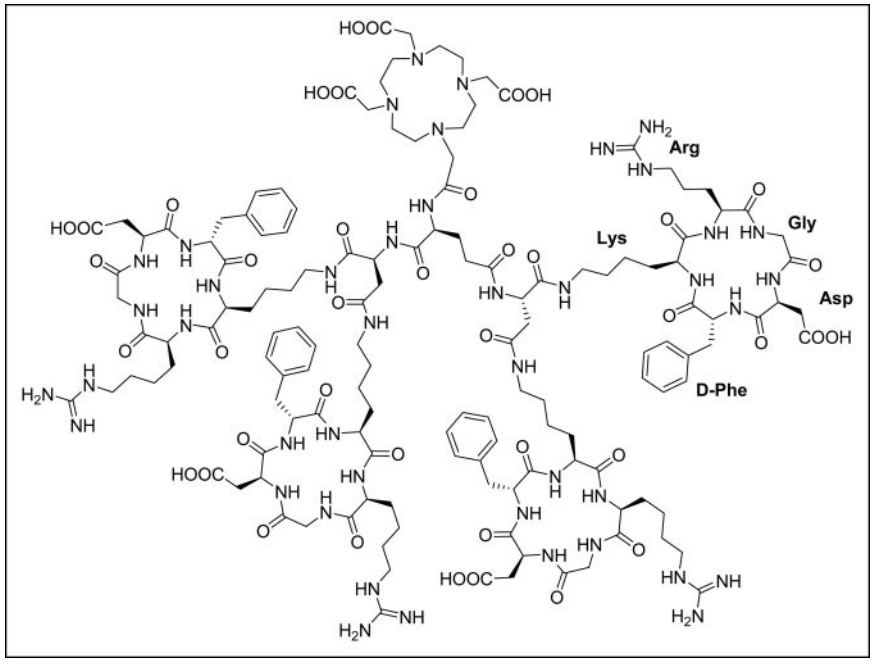

FIGURE 1. Schematic structure of DOTA-E{E[c(RGDfK)]$_2$}$_2$. The tetrameric RGD peptide was synthesized by coupling Boc-Glu(OSu)-OSu with dimeric RGD peptide E[c(RGDfK)]$_2$ followed by removal of Boc protecting group. DOTA conjugation was realized by reacting monoactive ester of DOTA with the free amino group on the N-terminal glutamate.

was activated with SNHS/EDC, and the resulting DOTA-OSSu ester was conjugated with tetrameric cyclic RGD peptide. The overall yield of DOTA-E{E[c(RGDfK)]$_2$}$_2$ was about 25% starting from Boc-Glu. ^{64}Cu labeling of DOTA-RGD tetramer conjugate was performed using ^{64}Cu having a measured specific activity of 1 Ci/μmol (37 MBq/nmol) at >95% radiochemical purity as determined by analytic HPLC (decay corrected). The ^{64}Cu-DOTA-E{E[c(RGDfK)]$_2$}$_2$ was purified by semipreparative HPLC. On the analytic HPLC, we observed no significant difference between ^{64}Cu-radiolabeled tracer and unlabeled conjugate. The tetrameric peptide tracer showed intermediate hydrophilicity, as indicated from octanol–water partition coefficient measurements, with a log *P* value of −1.60 ± 0.10.

Cell Integrin Receptor-Binding Assay

The receptor-binding affinity studies of DOTA-E{E[c(RGDfK)]$_2$}$_2$ for α_v integrin were performed using α_v integrin–positive U87MG cells rather than isolated receptors $\alpha_v\beta_3$. Binding on the cell membrane allows cross-linking and integrin receptor multimerization, by which multivalent binding and clustering of receptor is studied in the natural context of the integrin (*31*). We compared the receptor-binding affinity of DOTA conjugated tetrameric RGD peptide with that of unlabeled echistatin, E{E[c(RGDfK)]$_2$}$_2$, E[c(RGDfK)]$_2$, and DOTA-E[c(RGDfK)]$_2$ by performing competitive displacement studies with ^{125}I-echistatin (Fig. 2). All the peptides inhibited the binding of ^{125}I-echistatin to α_v integrin–positive U87MG cells. The IC_{50} values for echistatin, E{E[c(RGDfK)]$_2$}$_2$, and E[c(RGDfK)]$_2$, were 1.2 ± 0.1, 15.0 ± 1.1, and 32.2 ± 2.1 nmol/L, respectively. DOTA chelation had minimal effect on the receptor avidity of dimeric and tetrameric RGDs. The IC_{50} values for DOTA-E{E[c(RGDfK)]$_2$}$_2$ and DOTA-E[c(RGDfK)]$_2$ were 16.6 ± 1.3 and 48.4 ± 2.8 nmol/L, respectively. The cell-binding assay demonstrated that RGD tetramer had about 3-fold and almost 10-fold higher integrin avidity than the corresponding dimeric (*19*) and monomeric (*25*) RGD peptide analogs, respectively.

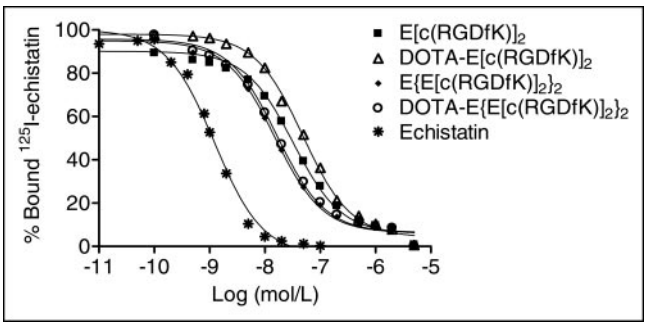

FIGURE 2. In vitro inhibition of ^{125}I-echistatin binding to α_v integrin on human glioblastoma cell line U87MG by echistatin, E[c(EGDfK)]$_2$, DOTA-E[c(EGDfK)]$_2$, E{E[c(RGDfK)]$_2$}$_2$, and DOTA-E{E[c(RGDfK)]$_2$}$_2$. Results are means of 3 experiments.

In Vivo Metabolism of ^{64}Cu-DOTA-E{E[c(RGDfK)]$_2$}$_2$

The metabolic stability of ^{64}Cu-DOTA-E{E[c(RGDfK)]$_2$}$_2$ was determined in mouse blood and urine and in liver and kidney homogenates at 30 min, 1 h, and 2 h after tracer injection. The extraction efficiency of all organs was between 65% and 100% (Fig. 3A). The lowest extraction efficiency was found for the kidney homogenates. Between 5% and 10% of the total activity could not be fixed on the C-18 cartridges, which can be related to very hydrophilic metabolites and protein-bound activity. The HPLC analyses of the soluble fraction of all organs and tissues allowed detection of only one major radiolabeled metabolite with the retention time between 3.3 to 4.0 min. The retention time for ^{64}Cu-DOTA-E{E[c(RGDfK)]$_2$}$_2$ was about 17.5 min (Fig. 3B). The tracer was stable in both blood (96.3% ± 3.5% intact tracer) and urine (95.3% ± 4.8% intact tracer) samples at 30 min after injection, but some degradation was found at late time points. The amount of intact tracer in the kidneys was approximately 70% at 30 min after injection and rapidly dropped to 21% over 2 h. This tracer in the liver showed rapid metabolism. Representative HPLC profiles of the soluble fractions of the different samples are shown in Figure 3C.

Biodistribution Studies

The biodistribution data of ^{64}Cu-DOTA-E{E[c(RGDfK)]$_2$}$_2$ in human U87MG glioma tumor-bearing athymic nude mice are shown in Figure 4A as the percentage administered activity (injected dose) per gram of tissue (%ID/g). This radiolabeled peptide displayed rapid blood clearance (0.61 ± 0.01 %ID/g at 30 min after injection and 0.21 ± 0.01 %ID/g at 4 h after injection). Rapid and high activity accumulation in the $\alpha_v\beta_3$-positive U87MG tumors was observed at early time points (9.93 ± 1.05 %ID/g at 30 min after injection). Tumor uptake slowly decreased to 7.61 ± 0.68 %ID/g at 2 h after injection, and 4.56 ± 0.51 %ID/g over 24 h. The biologic retention half-time $t_{1/2}$ of the ^{64}Cu-labeled tetrameric RGD peptide tracer was 4.3 h (R^2 = 0.99) in the tumor. The renal associated activity was initially high (9.02 ± 0.56 %ID/g, 30 min after injection), but fell to 2.83 ± 0.22 %ID/g at the end of 24 h (biologic retention $t_{1/2}$ = 1.72 h, R^2 = 0.99) (Table 1). Moderate liver activity accumulation (e.g., 4.38 ± 0.39 %ID/g at 1 h and 2.34 ± 0.18 %ID/g, respectively) was also observed at all times.

A receptor specificity was demonstrated by coinjection of c(RGDyK) (10 mg/kg), which is integrin $\alpha_v\beta_3$ positive, with ^{64}Cu-DOTA-E{E[c(RGDfK)]$_2$}$_2$ and measuring the biodistribution at 1 h after injection A significant decrease of radioactivity in all dissected tissues is shown in Figure 4B. Uptake in tumor was reduced most markedly from 9.70 %ID/g to 1.75 %ID/g. This experiment showed that the uptake and retention of ^{64}Cu-DOTA-E{E[c(RGDfK)]$_2$}$_2$ can be blocked in the presence of excess of nonradioactive RGD peptide in the U87MG tumor as well as in other organs, except blood and kidney. This simple blocking

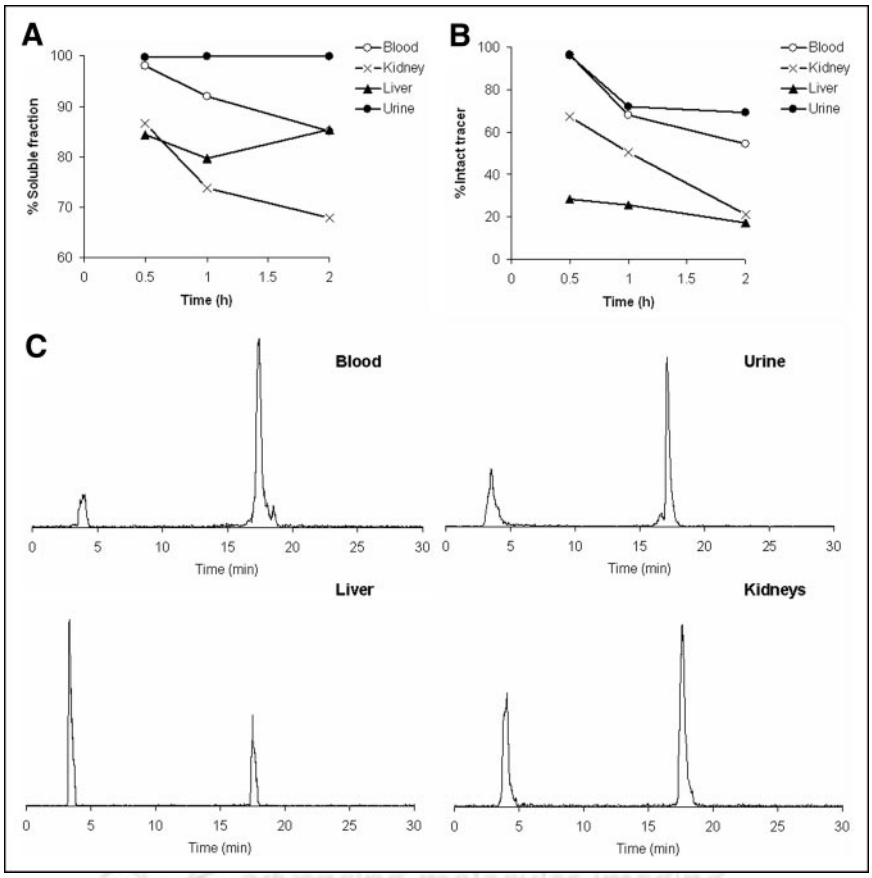

FIGURE 3. (A) Extraction efficiency of liver and kidney homogenates, blood, and urine samples at 30 min, 1 h, and 2 h after tracer injection in normal athymic nude mice ($n = 3$). (B) Time course of intact tracer in soluble fraction of blood, urine, and organ homogenates. (C) Representative HPLC elution profiles of soluble fraction of blood and urine samples, liver, and kidney homogenates collected 1 h after tracer injection.

experiment does not allow us to conclude with absolute certainty that tumor uptake of ^{64}Cu-DOTA-E{E[c(RGDfK)]$_2$}$_2$ is attributed to specific peptide–receptor interaction unless dose-dependent inhibition of tumor uptake is observed by coinjecting varying amounts of competing agents.

A comparison of the kinetics of excretion of ^{64}Cu-DOTA-E[c(RGDfK)]$_2$ and ^{64}Cu-DOTA-E{E[c(RGDfK)]$_2$}$_2$ from the blood, liver, kidneys, and U87MG tumors is shown in Figure 5. Both tracers demonstrated rapid blood clearance with the tetramer (biologic $t_{1/2} = 0.56$ h; $R^2 = 0.99$) slower than the dimer (biologic $t_{1/2} = 0.20$ h; $R^2 = 0.99$). The renal uptake of the tetramer was significantly higher than that of the dimer at all time points ($P < 0.0001$), presumably because of the charge differences of these 2 conjugates. No significant difference was seen between 2 tracers in the liver uptake at early time points ($P > 0.1$), but the tetramer displayed persistent activity accumulation in the liver while liver activity for the dimer was slowly excreted. The relatively lipophilic character of the cyclic RGDfK tetramer (log P = -1.6 ± 0.1) may be responsible for the hepatic residualization of this tracer. The uptake for ^{64}Cu-DOTA-E{E[c(RGDfK)]$_2$}$_2$ in the integrin-positive U87MG tumor was more than 2-fold higher than for ^{64}Cu-DOTA-E[c(RGDfK)]$_2$ ($P < 0.001$). Altogether, the prolonged tumor retention and rapid clearance from nontarget organs led to very high tumor-to-nontumor ratios for the tetrameric RGD peptide tracer (e.g., at 2 h time point, tumor-to-blood ratio = 34.8 ± 2.7; tumor-to-muscle ratio = 15.9 ± 1.2; tumor-to-liver ratio = 2.32 ± 0.18; tumor-to-kidney ratio = 1.54 ± 0.12; and tumor-to-small intestine ratio = 3.95 ± 0.30).

microPET Studies

The localization of ^{64}Cu-DOTA-E{E[c(RGDfK)]$_2$}$_2$ in human U87MG tumor-bearing nude mice ($n = 3$) was performed by multiple time-point static microPET scans. Figure 6A shows coronal microPET images of a female mouse at different times after injection following administration of 9.1 MBq (245 μCi) of the radiotracer. All microPET images were decay corrected. The tumor was clearly visualized with high tumor-to-contralateral background contrast, with the ratio higher than 5 at all times examined. Quantification of activity accumulation in the tumor and major organs (Fig. 6B) agreed well with that obtained from direct tissue sampling, except that the tumor-to-muscle ratio obtained from microPET was lower than that from biodis-

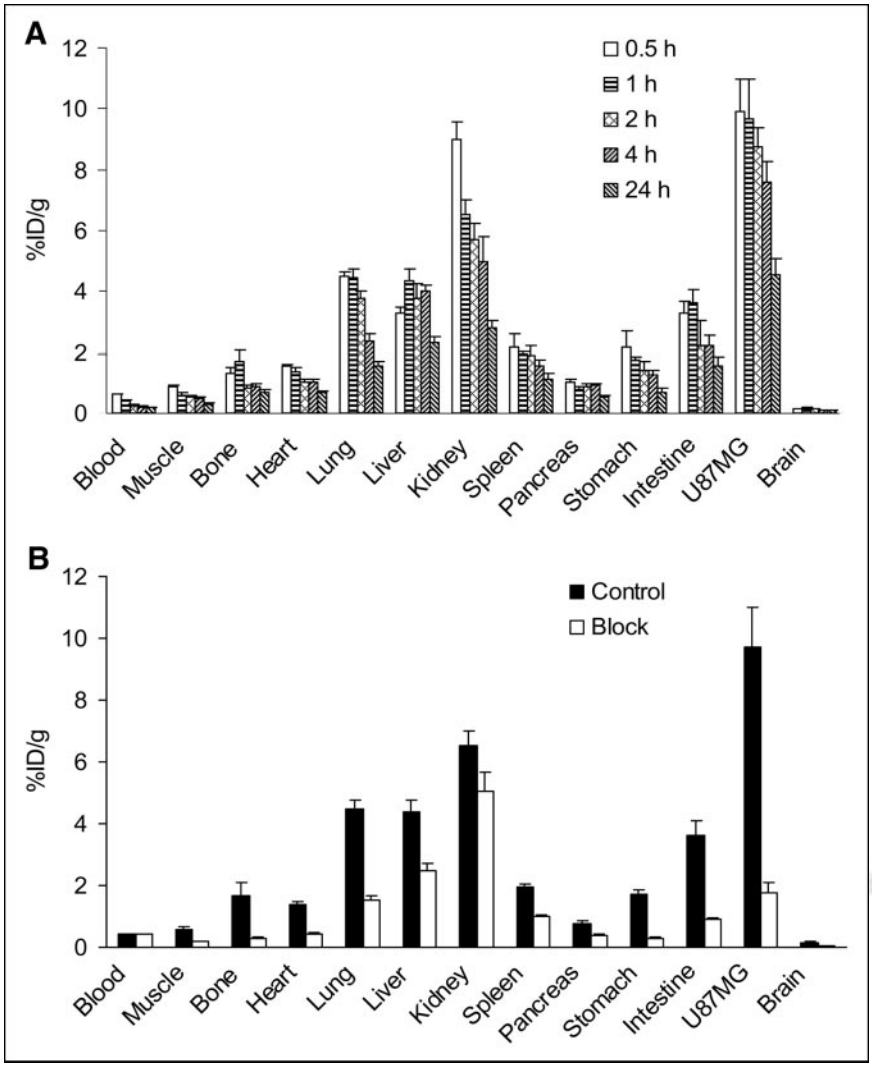

FIGURE 4. (A) Biodistribution data for ^{64}Cu-DOTA-E{E[c(RGDfK)]$_2$}$_2$ in athymic nude mice bearing subcutaneously xeno-transplanted U87MG tumors. Data are expressed as normalized accumulation of activity in %ID/g ± SD (n = 3). (B) Biodistributions of ^{64}Cu-DOTA-E{E[c(RGDfK)]$_2$}$_2$ in U87MG tumor-bearing athymic nude mice at 1 h with and without coinjection of 10 mg/kg of c(RGDyK) as a blocking agent (n = 3).

tribution studies ($P < 0.002$). No activity accumulation was observed in the normal brain, presumably because of a low α_v integrin expression level and an intact blood–brain barrier (BBB). Comparison of tumor uptakes in mice with and without coinjection of blocking dose of nonradioactive RGD peptide c(RGDyK) is illustrated in Figure 6C. Tumor-to-background contrasts at 1 h after injection for the control group and blocked group were 8.7 ± 1.5 and 2.3 ± 0.6, respectively.

Radiation Dosimetry

Table 1 shows the fractional uptake at time zero together with the biologic half-times for each organ of the mouse based on monoexponential clearance. Also shown are the biologic half-times and applicable fractions for the remainder of body based on a biexponential clearance function. The fractional uptakes (%ID) were greatest for the urinary bladder, tumor, and liver. These parameters were used to project radiation-absorbed doses per unit administered activity in an adult human (Table 2). These results predict that the highest radiation-absorbed doses will be to the urinary

TABLE 1
Average Fractional Uptake at Time Zero and Biologic Half-Times for Each Organ of Tumor-Bearing Mice According to Biodistribution Data (n = 3)

Organ	Fractional uptake (%)	Biologic half-times (h)
Heart	0.19	3.52
Lung	0.76	3.11
Liver	3.48	10.45
Kidneys	2.49	2.95
Spleen	0.19	6.00
Pancreas	0.09	9.32
Brain	0.05	8.52
Urine*†	25.0	0.05; 1.85
Remainder of body*	9.2	0.07; 4.40

*Biologic half-times were calculated based on a biexponential clearance function.
†Urinary bladder fraction calculated assuming no excretion.

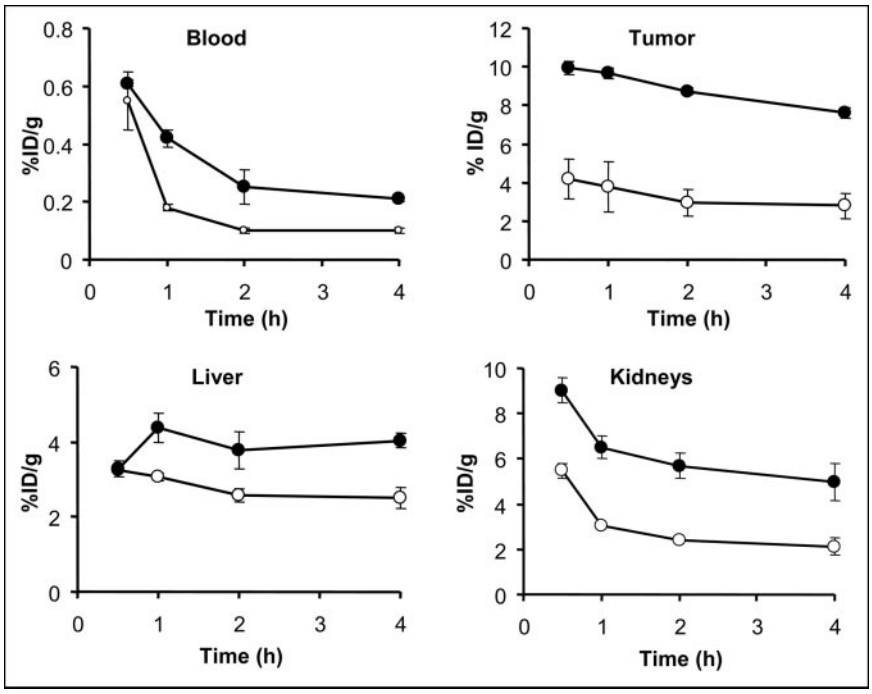

FIGURE 5. Comparison of biodistributions of ^{64}Cu-DOTA-E{E[c(RGDfK)]$_2$}$_2$ (●) and ^{64}Cu-DOTA-E[c(RGDfK)]$_2$ (○) in U87MG tumor-bearing athymic nude mice. Error bars denote SDs (n = 3).

bladder wall (0.262 mGy/MBq), kidneys (0.0296 mGy/MBq), and liver (0.0242 mGy/MBq). The whole-body absorbed dose was found to be 0.0164 mSv/MBq administered.

DISCUSSION

This study describes the synthesis of a tetrameric RGD peptide ligand for radiolabeling with the positron-emitting radionuclide ^{64}Cu for imaging tumor integrin expression. The new tracer ^{64}Cu-DOTA-E{E[c(RGDfK)]$_2$}$_2$ (Fig. 1) shows a very high tumor-to-nontumor contrast and should be useful for targeted diagnosis and radiotherapy of integrin $\alpha_v\beta_3$–positive tumors.

A variety of radiolabeled peptides are being evaluated for tumor localization and therapy. Radiolabeled RGD peptides are of particular interest because they bind to the integrin $\alpha_v\beta_3$ overexpressed on newly formed blood vessels and cells of many common cancer types. However, most small cyclic RGD peptides tracers result in fast blood clearance accompanied by low tumor uptake and rapid tumor washout, presumably due to suboptimal receptor-binding affinity and inadequate contact with cell-surface integrin receptors (*17,24–29,32–34*).

We and others (*18–23*) have previously applied the concept of bivalency to develop dimeric RGD peptides for improved tumor targeting over that of the corresponding monomeric RGD peptide analogs. In principle, the introduction of the homogeneous dimeric RGD peptide system is expected to improve integrin targeting by cooperative receptor interactions and receptor shielding to endogenous competition. Dimeric RGD peptide E[c(RGDfK)]$_2$ was conjugated with DOTA or HYNIC, which enables labeling with ^{111}In (*21*), ^{90}Y (*21,23*), ^{64}Cu (*19*), and ^{99m}Tc (*18,22*). The dimeric RGD peptide tracer showed higher receptor-binding affinity and specificity for integrin $\alpha_v\beta_3$ in vitro and enhanced tumor uptake and retention in vivo as compared with the monomeric RGD peptide analog. A single injection of ^{90}Y-DOTA-E[c(RGDfK)]$_2$ at maximum tolerated dose caused a significant delay in tumor growth in a small subcutaneous OVCAR-3 ovarian xenograft tumor model (*21*). We found that replacing D-phenylalanine with D-tyrosine increased the hydrophilicity of the dimeric RGD peptide and, consequently, resulted in increased integrin-mediated tumor uptake and more favorable biokinetics in an orthotopic MDA-MB-435 breast cancer model (*19*). E[c(RGDyK)]$_2$ was also labeled with ^{18}F by using a prosthetic 4-^{18}F-fluorobenzoyl group and showed significantly higher tumor uptake and prolonged tumor retention in comparison with the ^{18}F-labeled monomeric RGD peptide because of the synergistic effect of bivalency and improved pharmacokinetics (*20*).

Although the dimeric RGD peptide tracers had some incremental improvement on tumor targeting and pharmacokinetics as compared with the monomeric RGD peptide analogs, the intermediate tumor uptake and persistent renal activity accumulation of this type of radioligand prevent their translation into human beings for diagnostic or therapeutic applications.

We hypothesize that multimerization to introduce tetrameric RGD peptides might further increase the re-

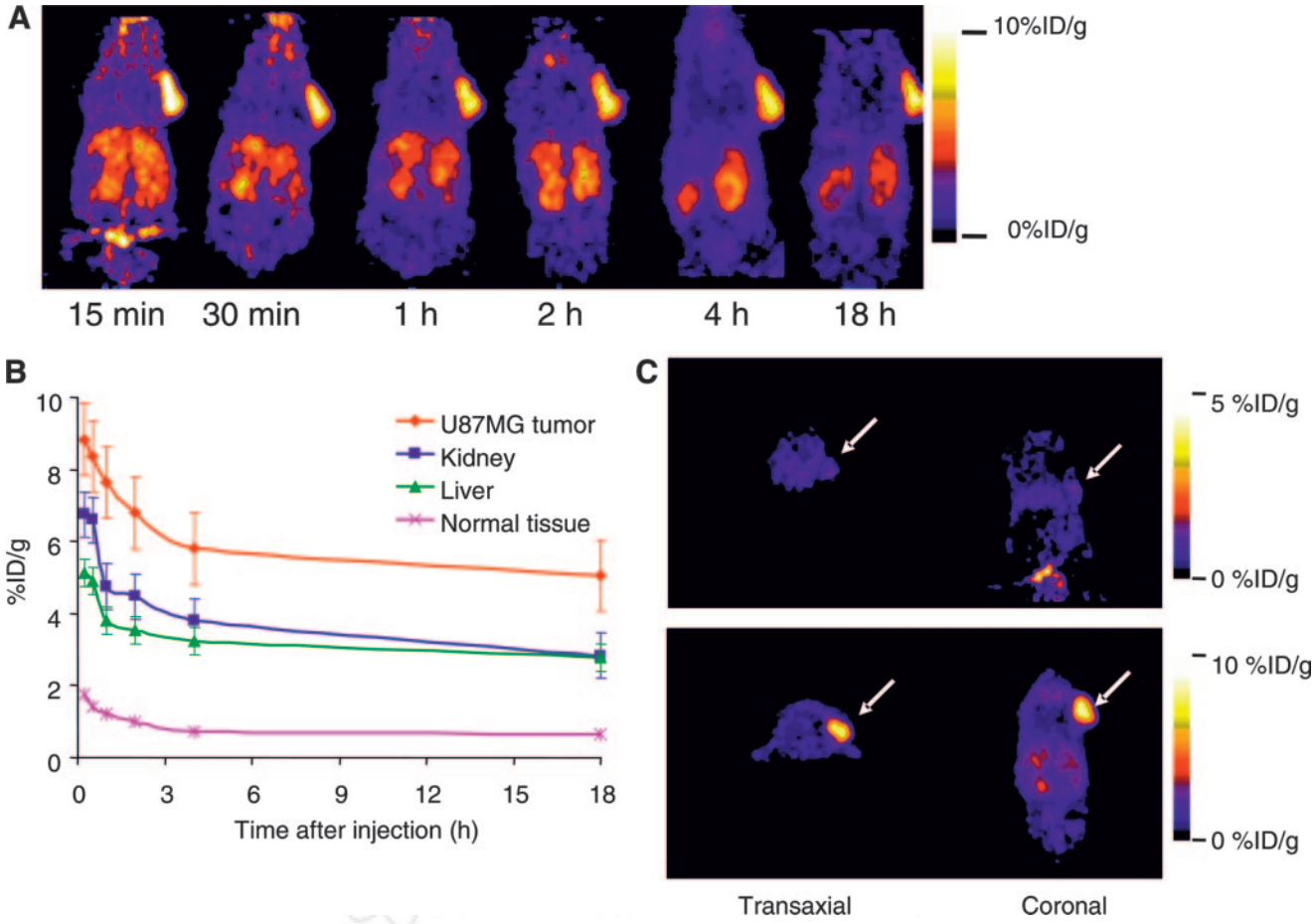

FIGURE 6. (A) Decay-corrected whole-body coronal microPET images of nude mouse bearing human U87MG tumor at 15 and 30 min and at 1, 2, 4, and 18 h (10-min static image) after injection of 9.1 MBq (245 μCi) of ^{64}Cu-DOTA-E{E[c(RGDfK)]$_2$}$_2$. (B) Time–activity curves derived from multiple time-point microPET study. ROIs are shown as the mean %ID/g ± SD (n = 4). (C) Comparison of tumor uptakes in mice injected with ^{64}Cu-DOTA-E{E[c(RGDfK)]$_2$}$_2$ at a dose of 9.3 MBq with (top) or without (bottom) 10 mg/kg c(RGDyK).

ceptor-binding affinity presumably because of the polyvalency effect. In this study, we designed a new tetrameric RGD peptide with repeating c(RGDfK) units connected through glutamate linkers. A cell receptor–binding assay using integrin-positive U87MG cells and ^{125}I-echistatin as the radioligand found integrin avidity of E{E[c(RGDfK)]$_2$}$_2$ > E[c(RGDfK)]$_2$ > c(RGDfK) (Fig. 2). DOTA conjugation had a minimal effect on the integrin affinity of the RGD peptides. When applied to the subcutaneous U87MG glioblastoma xenogarft model, ^{64}Cu-DOTA-E{E[c(RGDfK)]$_2$}$_2$ showed high tumor uptake and primarily renal and secondarily hepatic excretion routes (Figs. 4 and 6). The initial high tumor uptake might be attributed to the high integrin affinity of the tracer. The increased molecular size resulting in longer blood circulation time might be responsible for the prolonged tumor retention. At any given time, the in vivo tumor signal not only is attributed to specific binding but also presents contributions from nonspecific binding, free ligand in tissue, and intravascular activity. Kinetic modeling (e.g., Logan plot) (*35*) of the noninvasive dynamic PET data may be applied to directly measure affinity constants and binding potential in vivo.

Kidney retention of ^{64}Cu was much longer for ^{64}Cu-DOTA-E{E[c(RGDfK)]$_2$}$_2$ than for ^{64}Cu-DOTA-E[c(RGDfK)]$_2$ (Fig. 5). Differences in renal uptake and excretion may be related to the charge differences of these 2 conjugates. The tetrameric RGD peptide tracer is more positively charged than the dimeric RGD peptide tracer because of the presence of more secondary amino groups, similar to what is observed for the difference between dimers and monomers (*18–23*). The positively charged radiopeptides or metabolites are usually retained in the kidney after resorption by renal tubular cells and lysosomal proteolysis (*36*). We also note from Figure 5 that the enhanced tumor uptake of the tetramer compared with the dimer is accompanied by a similar increase in renal uptake. Thus, tumor-to-kidney ratios do not increase significantly when using the tetrameric RGD peptide tracer and, consequently, the therapeutic window may not be increased and the advantage of a tetramer over a dimer might be modest. Blocking cationic binding sites in the kidneys

TABLE 2
Estimated Radiation-Absorbed Doses to Adult Human After Intravenous Injection of ^{64}Cu-DOTA-E{E[c(RGDfK)]$_2$}$_2$ Based on Average Biodistribution Data Obtained in U87MG Glioblastoma-Bearing Nude Mice (n = 3)

Target organ	mGy/MBq (SD)	rad/mCi (SD)
Adrenals	2.07E−03 (3.31E−04)	7.67E−03 (1.23E−03)
Brain	4.73E−04 (3.64E−05)	1.75E−03 (1.35E−04)
Breasts	6.58E−04 (1.05E−04)	2.43E−03 (3.89E−04)
Gallbladder wall	3.00E−03 (4.80E−04)	1.11E−02 (1.78E−03)
Lower large intestine	3.94E−03 (6.30E−04)	1.46E−02 (2.34E−03)
Small intestine	2.19E−03 (3.50E−04)	8.10E−03 (1.30E−03)
Stomach wall	1.28E−03 (2.05E−04)	4.74E−03 (7.58E−04)
Upper large intestine	2.04E−03 (3.26E−04)	7.53E−03 (1.20E−03)
Heart wall	3.22E−03 (6.15E−05)	1.19E−02 (2.27E−04)
Kidneys	2.96E−02 (1.84E−03)	1.10E−01 (6.84E−03)
Liver	2.43E−02 (1.56E−03)	8.98E−02 (5.76E−03)
Lungs	9.57E−04 (2.34E−05)	3.54E−03 (8.66E−05)
Muscle	1.55E−03 (8.90E−05)	5.74E−03 (3.30E−04)
Ovaries	3.74E−03 (5.98E−04)	1.38E−02 (2.21E−03)
Pancreas	1.15E−02 (4.73E−04)	4.24E−02 (1.74E−03)
Red marrow	1.28E−03 (2.05E−04)	4.75E−03 (7.60E−04)
Osteogenic cells	1.46E−03 (2.34E−04)	5.41E−03 (8.66E−04)
Skin	8.32E−04 (1.33E−04)	3.08E−03 (4.93E−04)
Spleen	8.16E−03 (1.64E−03)	3.02E−02 (6.07E−03)
Testes	2.72E−03 (4.35E−04)	1.01E−02 (1.62E−03)
Thymus	6.80E−04 (1.09E−04)	2.51E−03 (4.02E−04)
Thyroid	5.05E−04 (8.08E−05)	1.87E−03 (2.99E−04)
Urinary bladder wall	2.62E−01 (4.72E−02)	9.69E−01 (1.75E−01)
Uterus	7.92E−03 (1.27E−03)	2.93E−02 (4.69E−03)
Total body dose	2.35E−03 (3.76E−04)	8.69E−03 (1.39E−03)
Effective dose*	1.64E−02 (2.95E−03)	6.06E−02 (1.09E−02)

*In unit of mSv/MBq or rem/mCi.

snm advancing molecular imaging

with cationic amino acid infusion was reported to reduce renal uptake without compromising the tumor activity accumulation in both mice and humans (*37*). We expect that renal uptake of ^{64}Cu-DOTA-E{E[c(RGDfK)]$_2$}$_2$ may be blocked by coadministration of D- or L-lysines (*37*). Modification of DOTA-E{E[c(RGDfK)]$_2$}$_2$ conjugation by inserting a pharmacokinetic modifier to make the ^{64}Cu-labeled complex neutral or negatively charged may also improve the biokinetics of the tracer. Tetrameric RGD peptide tracer had moderate but persistent liver uptake. Although the factors that exert this influence are not fully understood, it is clear that the charge, lipophilicity, and stability of the copper complex play major roles. Our pervious experience with ^{64}Cu-labeled dimeric RGD peptide found that replacing D-Phe with D-Tyr increased the hydrophilicity of the resulting radiotracer and subsequently reduced liver uptake (*19*). We suggest that ^{64}Cu-DOTA-E{E[c(RGDyK)]$_2$}$_2$ may exhibit less liver uptake than ^{64}Cu-DOTA-E{E[c(RGDfK)]$_2$}$_2$.

In addition to U87MG tumor, ^{64}Cu-labeled RGD tetramer uptake in some normal organs and tissues was also inhibited by coadministration of an excess amount of monomeric RGD peptide c(RGDyK) (Fig. 4B). Western blot analysis of the tissue lysates suggested that these organs express a low amount of integrin $\alpha_v\beta_3$ (data not shown). Whether integrin-mediated localization of ^{64}Cu-DOTA-E{E[c(RGDyK)]$_2$}$_2$ in nontumor tissues will affect its imaging as well therapeutic application requires further investigation.

The OLINDA software (*30*), as a replacement for MIRDOSE3, provides a calculation of the effective dose for human adults as defined in ICRP Publication 60 (*38*). The urinary bladder received the highest absorbed doses, reflecting rapid clearance of most of the injected ^{64}Cu-DOTA-E{E[c(RGDyK)]$_2$}$_2$ into the bladder and making it the limiting organ as far as the amount of ^{64}Cu-DOTA-E{E[c(RGDyK)]$_2$}$_2$ that can be injected. However, the patient's voiding interval affects the radiation dose absorbed by the urinary bladder and, because the urinary bladder is the limiting organ, the patient's frequency of urination will change the bladder dose. Previous nonhuman primate imaging studies with ^{64}Cu-labeled octreotide ^{64}Cu-TETA-Y3-TATE found that the bladder dose could be reduced >7-fold by a normal voiding scheme as compared with no excretion assumption (*39*). If this is also true for our tetrameric RGD peptide tracer, then the kidneys appear to be the most affected and dose-limiting organs in human studies with regard to toxicity. The human kidney and liver doses of ^{64}Cu-DOTA-E{E[c(RGDfK)]$_2$}$_2$ calculated from mouse biodistribution data (0.030 and 0.024 mGy/MBq, respec-

tively) were significantly lower than those of ^{64}Cu-labeled octreotide ^{64}Cu-DOTA-OC calculated from clinical PET (0.078 and 0.091 mGy/MBq, respectively) (*40*). The use of rodent biodistribution data is generally thought to give a worst-scenario estimate of absorbed doses to normal organs. Whether this is true for ^{64}Cu-DOTA-E{E[c(RGDfK)]$_2$}$_2$ remains to be tested in human patients. Nevertheless, methods to decrease the uptake of radioligand in the kidneys, such as coadministration of cationic amino acids (*37*) or modifying the structure to render the overall neutral or negatively charged molecule, may be able to minimize long-term damage to this organ if a particle ray-emitting isotope is used for the therapy.

Previous clinical investigations demonstrated the expression of integrin $\alpha_v\beta_3$ in glioma-associated angiogenesis (*11*). We have also shown that both subcutaneous and orthotopic U87MG glioblastoma xenografts (*20,24,26,27*) had high level of integrin. However, the subcutaneous tumor model used in this study does not accurately represent the growth, invasion, histology, gene expression profiling, vasculature, and stromal interactions or intracranial tumors.

In addition, the tumor model from the established U87MG glioblastoma cell line does not necessarily reflect the biology, heterogeneity, or therapeutic response of the primary tumor from which it was derived. Genetically accurate animal models for brain tumors such as those described in the Mouse Models of Human Cancers Consortium (MMHCC) (http://emice.nci.nih.gov/) that are more likely to parallel the human situation may be used in the future to test the clinical potential of the tetrameric RGD peptide tracer.

CONCLUSION

^{64}Cu-DOTA-E{E[c(RGDfK)]$_2$}$_2$ was shown to bind with high affinity and specificity with integrin-positive U87MG glioma cells in vitro and in vivo and has the right characteristics for further pursuit as an imaging agent with PET. The presumed polyvalency effect and suitable apparent size of this tetrameric RGD peptide tracer make it a superior ligand for integrin targeting in vivo. Although the effectiveness of this copper complex to eradicate integrin-positive tumors was untested, high and prolonged tumor uptake and favorable pharmacokinetics suggest that the this tetrameric RGD peptide tracer has great potential as a clinical PET radiopharmaceutical for imaging tumor integrin expression and as a therapeutic radiopharmaceutical to treat integrin-positive tumors. Because DOTA is a universal chelator capable of forming stable complexes with a variety of metals, such as ^{111}In, $^{67/68}$Ga, $^{64/67}$Cu, $^{86/90}$Y, and ^{177}Lu, the same peptide conjugate used for ^{64}Cu labeling in this study can also be applied to label other radiometals for tumor localization and therapy.

ACKNOWLEDGMENTS

This work was supported, in part, by National Institute of Biomedical Imaging and Bioengineering grant R21 EB001785, Department of Defense (DOD) Breast Cancer Research Program (BCRP) Concept Award DAMD17-03-1-0752, DOD BCRP IDEA Award W81XWH-04-1-0697, DOD Prostate Cancer Research Program New Investigator Award DAMD1717-03-1-0143, the American Lung Association California (ALAC), the Society of Nuclear Medicine Education and Research Foundation, and National Cancer Institute (NCI) Small Animal Imaging Resource Program R24 CA93862. The production of ^{64}Cu at Washington University School of Medicine is supported by NCI grant R24 CA86307.

REFERENCES

1. Davis FG, Freels S, Grutsch J, Barlas S, Brem S. Survival rates in patients with primary malignant brain tumors stratified by patient age and tumor histological type: an analysis based on Surveillance, Epidemiology, and End Results (SEER) data, 1973–1991. *J Neurosurg.* 1998;88:1–10.
2. Jemal A, Tiwari RC, Murray T, et al. Cancer statistics, 2004. *CA Cancer J Clin.* 2004;54:8–29.
3. Grossman SA, Batara JF. Current management of glioblastoma multiforme. *Semin Oncol.* 2004;31:635–644.
4. Folkman J. Role of angiogenesis in tumor growth and metastasis. *Semin Oncol.* 2002;29:15–18.
5. Brook PC, Clark RAF, Cheresh DA. Requirement of vascular integrin $\alpha_v\beta_3$ for angiogenesis. *Science.* 1994;264:569–571.
6. Puduvali VK. Inhibition of angiogenesis as a therapeutic strategy against brain tumor. *Cancer Treat Res.* 2004;117:307–336.
7. Friedlander M, Brooks PC, Shiller RW, Kincaid CH, Varner JA, Cheresh DA. Definition of two angiogenic pathways by distinct α_v integrin. *Science.* 1995; 270:1500–1502.
8. Horton MA. The $\alpha_v\beta_3$ integrin "vitronectin receptor". *Int J Biochem Cell Biol.* 1997;29:721–725.
9. Brooks PC, Montgomery AM, Rosenfeld M, et al. Integrin $\alpha_v\beta_3$ antagonists promote tumor regression by inducing apoptosis of angiogenic blood vessels. *Cell.* 1994;79:1157–1164.
10. Hwang R, Varner JV. The role of integrins in tumor angiogenesis. *Hematol Oncol Clin North Am.* 2004;18:991–1006.
11. Bello L, Francolini M, Marthyn P, et al. $\alpha_v\beta_3$ and $\alpha_v\beta_5$ integrin expression in glioma periphery. *Neurosurgery.* 2001;49:380–390.
12. Jin H, Varner J. Integrins: roles in cancer development and as treatment targets. *Br J Cancer.* 2004;90:561–565.
13. Kumar CC. Integrin $\alpha_v\beta_3$ as a therapeutic target for blocking tumor-induced angiogenesis. *Curr Drug Targets.* 2003;4:123–131.
14. Sipkins DA, Cheresh DA, Kazemi MR, Nevin LM, Bednarski MD, Li KC. Detection of tumor angiogenesis *in vivo* by $\alpha_v\beta_3$-targeted magnetic resonance imaging. *Nat Med.* 1998;4:623–626.
15. Ellegala DB, Leong-Poi H, Carpenter JE, et al. Imaging tumor angiogenesis with contrast ultrasound and microbubbles targeted to $\alpha_v\beta_3$. *Circulation.* 2003;108: 336–341.
16. Chen X, Conti PS, Moats RA. In vivo near-infrared fluorescence imaging of integrin $\alpha_v\beta_3$ in brain tumor xenografts. *Cancer Res.* 2004;64:8009–8014.
17. Haubner R, Wester HJ. Radiolabeled tracers for imaging of tumor angiogenesis and evaluation of anti-angiogenic therapies. *Curr Pharm Des.* 2004;10:1439–1455.
18. Liu S, Edwards DS, Ziegler MC, Harris AR, Hemingway SJ, Barrett JA. ^{99m}Tc-Labeling of a hydrazinonicotinamide-conjugated vitronectin receptor antagonist useful for imaging tumors. *Bioconjug Chem.* 2001;12:624–629.
19. Chen X, Liu S, Hou Y, et al. MicroPET imaging of breast cancer α_v-integrin expression with ^{64}Cu-labeled dimeric RGD peptides. *Mol Imaging Biol.* 2004;6: 350–359.
20. Chen X, Tohme M, Park R, Hou Y, Bading JR, Conti PS. Micro-PET imaging of $\alpha_v\beta_3$-integrin expression with ^{18}F-labeled dimeric RGD peptide. *Mol Imaging.* 2004;3:96–104.
21. Janssen ML, Oyen WJ, Dijkgraaf I, et al. Tumor targeting with radiolabeled $\alpha_v\beta_3$

integrin binding peptides in a nude mouse model. *Cancer Res.* 2002;62:6146–6151.
22. Janssen M, Oyen WJ, Massuger LF, et al. Comparison of a monomeric and dimeric radiolabeled RGD-peptide for tumor targeting. *Cancer Biother Radiopharm.* 2002;17:641–646.
23. Janssen M, Frielink C, Dijkgraaf I, et al. Improved tumor targeting of radiolabeled RGD peptides using rapid dose fractionation. *Cancer Biother Radiopharm.* 2004;19:399–404.
24. Chen X, Park R, Shahinian AH, Bading JR, Conti PS. Pharmacokinetics and tumor retention of ^{125}I-labeled RGD peptide are improved by PEGylation. *Nucl Med Biol.* 2004;31:11–19.
25. Chen X, Park R, Tohme M, Shahinian AH, Bading JR, Conti PS. MicroPET and autoradiographic imaging of breast cancer α_v-integrin expression using ^{18}F- and ^{64}Cu-labeled RGD peptide. *Bioconjug Chem.* 2004;15:41–49.
26. Chen X, Park R, Shahinian AH, et al. ^{18}F-Labeled RGD peptide: initial evaluation for imaging brain tumor angiogenesis. *Nucl Med Biol.* 2004;31:179–189.
27. Chen X, Hou Y, Tohme M, et al. Pegylated Arg-Gly-Asp peptide: ^{64}Cu labeling and PET imaging of brain tumor $\alpha_v\beta_3$-integrin expression. *J Nucl Med.* 2004;45:1776–1783.
28. Chen X, Sievers E, Hou Y, et al. Integrin $\alpha_v\beta_3$-targeted imaging of lung cancer. *Neoplasia.* 2005;7:271–279.
29. Haubner R, Kuhnast B, Mang C, et al. [^{18}F]Galacto-RGD: synthesis, radiolabeling, metabolic stability, and radiation dose estimates. *Bioconjug Chem.* 2004;15:61–69.
30. Sgouros G. Dosimetry of internal emitters. *J Nucl Med.* 2005;46(suppl):18S–27S.
31. Hynes RO. Integrins: bidirectional, allosteric signaling machines. *Cell.* 2002;110:673–687.
32. Haubner R, Wester HJ, Burkhart F, et al. Glycosylated RGD-containing peptides: tracer for tumor targeting and angiogenesis imaging with improved biokinetics. *J Nucl Med.* 2001;42:326–336.
33. Haubner R, Wester HJ, Weber WA, et al. Noninvasive imaging of $\alpha_v\beta_3$ integrin expression using ^{18}F-labeled RGD-containing glycopeptide and positron emission tomography. *Cancer Res.* 2001;61:1781–1785.
34. van Hagen PM, Breeman WA, Bernard HF, et al. Evaluation of a radiolabelled cyclic DTPA-RGD analogue for tumour imaging and radionuclide therapy. *Int J Cancer.* 2000;90:186–198.
35. Logan J. Graphical analysis of PET data applied to reversible and irreversible tracers. *Nucl Med Biol.* 2000;27:661–670.
36. Akizawa H, Arano Y, Mifune M, et al. Effect of molecular charges on renal uptake of ^{111}In-DTPA-conjugated peptides. *Nucl Med Biol.* 2001;28:761–768.
37. Jamar F, Barone R, Mathieu I, et al. ^{86}Y-DOTA-D-Phe^1-Tyr^3-octreotide (SMT487): a phase 1 clinical study—pharmacokinetics, biodistribution and renal protective effect of different regimens of amino acid co-infusion. *Eur J Nucl Med Mol Imaging.* 2003;30:510–518.
38. International Commission on Radiological Protection. 1990 Recommendations of the International Commission on Radiological Protection: ICRP Publication 60. *Ann ICRP.* 1991;21:6–10.
39. Lewis JS, Lewis MR, Cutler PD, et al. Radiotherapy and dosimetry of ^{64}Cu-TETA-Tyr^3-octreotate in a somatostatin receptor-positive, tumor-bearing rat model. *Clin Cancer Res.* 1999;5:3608–3616.
40. Anderson CJ, Dehdashti F, Cutler PD, et al. ^{64}Cu-TETA-octreotide as a PET imaging agent for patients with neuroendocrine tumors. *J Nucl Med.* 2001;42:213–221.

snm
advancing molecular imaging